2021

A Generalized Approach for Automated Compressor Performance Mapping Using Artificial Neural Network

Jie Ma
Purdue University, ma319@purdue.edu

Xin Ding

W. Travis Horton

Davide Ziviani

A Generalized Approach for Automated Compressor Performance Mapping Using Artificial Neural Network

Jie MA[1], Xin DING[1], W. Travis HORTON[1], Davide ZIVIANI[1]

[1]Ray W. Herrick Laboratories, School of Mechanical Engineering, Purdue University
West Lafayette, 47907-2099, USA
ma319@purdue.edu; wthorton@purdue.edu; dziviani@purdue.edu

ABSTRACT

In the last decades, several research and development efforts led to new compressor technologies that have been successfully introduced into market such as hermetic compressors with variable-speed motors, compressors with economization lines (both vapor and liquid injection lines), hermetic linear compressors, novel capacity modulations, and oil-flooding among others. During the process of implementing new compressor technologies, performance mapping is essential to predict the system behavior across different operating conditions. However, current standard AHRI-540 for compressor performance rating utilizes a 10-coefficient polynomial model that has severe limitations to include compressor enhancement technologies and variable operating range. In addition, it is common practice in industry to calibrate such polynomial correlations with at least 15 to 20 compressor calorimeter test points for a single compressor to ensure a good fit, which results in extended laboratory testing time and relatively high associated costs. Therefore, an automated compressor performance mapping approach based on artificial neural network (ANN) modeling is proposed to address and overcome the limitations of the current standard including applicability to any positive displacement compressors and minimization of number of test points required to accurately predict the compressor envelope.

In this paper, the performance of a positive displacement compressor is mapped by this novel methodology, which relies on an algorithm that effectively determines the minimum set of data points required and optimizes the training/testing of ANN architecture. The accuracy and reliability of the proposed methodology are compared to the conventional 10-coefficient polynomial mapping. Lastly, the propagated uncertainties through the model and its extrapolation capabilities are also analyzed.

Keywords: compressor performance mapping, calorimeter testing, artificial neuron network

1. INTRODUCTION

Improving the performance of air-conditioning and heat pumping (ACHP) systems to address space conditioning requirements, energy savings, and environmental concerns is a particularly challenging task. Research and development efforts at both component and system levels are continuously being pursued by both industry and academia. In order to evaluate the performance of different types of compressors and predict their behaviors within systems, various mathematical models have been proposed in the literature. In industry, it is a common practice to apply current ANSI/AHRI Standard 540 (AHRI, 2015) for compressor performance rating and utilize the 10-coefficient cubic polynomial model to predict the mass flow rate and compressor power. However, to ensure a good fit, at least 15 to 20 compressor calorimeter test points are need for a single compressor and that requires extended laboratory testing time. In academic, empirical and semi-empirical models including plenty physical information have been widely used to map compressor performance and extrapolate results, which is usually suitable for compressor research and design. But this physical-based model cannot be applied for various types of compressor and is relatively cumbersome for industrial application.

In order to overcome these limitations and improve the current methodology for compressor performance map rating, a novel approach of an automated compressor performance mapping approach based on ANN modeling has been developed and proposed by Ma et al., (2020) . They applied this methodology on three different types of compressors and compared the accuracy of ANN model to 10-coefficiency polynomial model. Ziviani et al., (2019) implemented a multi-input multi-out ANN model that can achieve higher accuracy with respect to a semi-empirical model to predict the performance of a single-phase and two-phase injected scroll compressor. In these works, it illustrates that the ANN model has significant potential and benefits on compressor performance mapping and rating.

In this paper, it is demonstrated the implementation of automated compressor performance mapping methodology based on ANN modeling with various set of training data points required and ANN architecture for a hermetic dual-cylinder rolling-piston compressor. Furthermore, the accuracy and reliability of the proposed methodology are compared

to the conventional 10-coefficient polynomial mapping, and the propagated uncertainties through the model and its extrapolation capabilities are also analyzed.

2. METHODOLOGY

The overall automated compressor mapping methodology is illustrated in **Error! Reference source not found.**, which is proposed by Ma et al., (2020). It is assumed that the compressor envelope has been already identified first. Hence, the compressor colorimeter (or hot gas bypass) testing data within the envelope can be used to train and test the ANN model. This simplification is necessary in order to develop and test the proposed mapping algorithm. Since the number and quality of training data impact the accuracy of prediction dramatically, the determination the training and validation dataset is critical for model regression. With respect to selecting the initial training samples, Aute et al., (2015) suggested that initial training samples can be chosen to be the vertices of a compressor envelope polygon, or the points as close to envelope boundary as possible to capture the compressor operating envelope.

In ANN model, the inputs include the ambient temperature (T_{amb}), suction pressure (P_{suc}), suction temperature (T_{suc}), and discharge pressure (P_{dis}). Whereas, the outputs from the model are the discharge temperature (T_{dis}), mass flow rate of refrigerant ($\dot{m}_r$), and compressor power consumption ($\dot{W}_{comp}$). In additions, four or five data points are selected on the compressor envelope boundary as the initial training samples, which include the lowest and highest evaporating and condensing temperatures, respectively. These initial points also present the minimum and maximum values of the output variables. After creating a training dataset with minimum number of training samples, an ANN model with single-input-layer, single-hidden-layer and single-output-layer structure is trained to predict compressor performance through iterating the weights and biases values. Additionally, the remaining data samples are used for validation. The method of determining the initial training data and ANN model structure is based on the work presented by Ma et al., (2020).

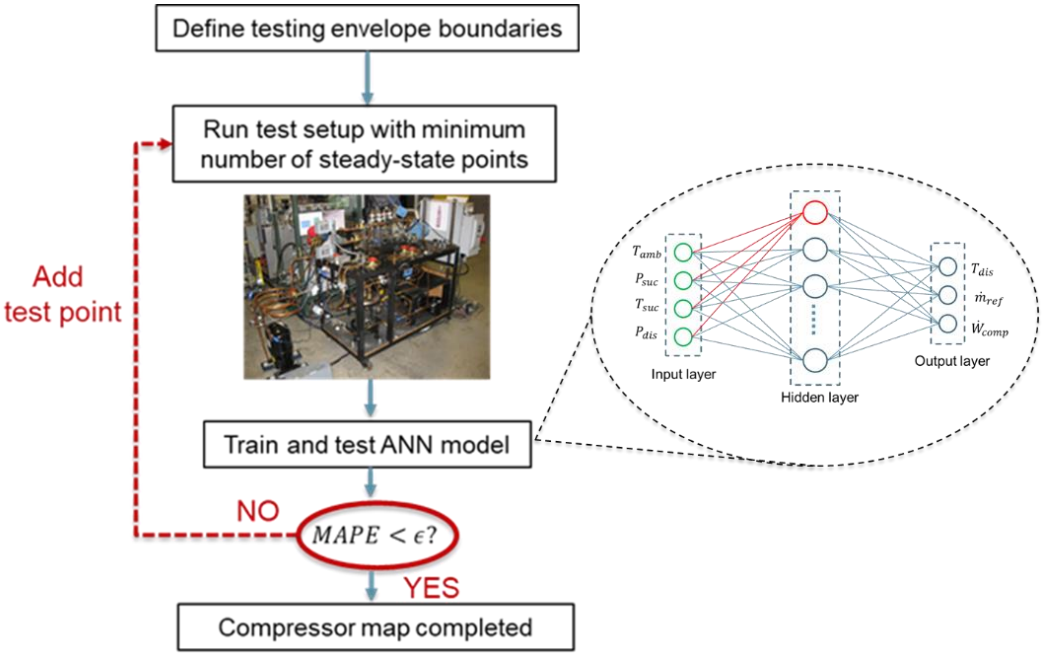

Figure 1: Conceptual schematic of the overall mapping methodology

To evaluate the accuracy of the trained ANN model, three well-known statistical quantities have been used introduced. The R^2 value is used to measure how statistically close the data are to the fitted regression line and is defined as:

$$R^2 = \frac{cov(y^{actual}, y^{predict})}{\sqrt{cov(y^{actual}, y^{actual})cov(y^{predict}, y^{predict})}} \tag{1}$$

where $cov(\cdot)$ denotes the covariance, y^{actual} is the actual experimental data, and $y^{predict}$ is the ANN model predicted data. Since the R^2 cannot determine whether the coefficient estimated and the predictions are biased, additional indicators are introduced. The mean absolute percentage error (MAPE) in Equation (2) is selected to statistically measure how accurate the ANN model.

$$MAPE = \frac{100\%}{n}\sum\left|\frac{y_i^{actual} - y_i^{predict}}{y_i^{actual}}\right| \tag{2}$$

3. COMPRESSOR MAPPING MODELS

3.1 AHRI 10-coefficient mapping and ANN models

The proposed compressor mapping approach is applied to a hermetic dual-cylinder rolling-piston compressor with R410A as the working fluid. A total of 43 steady-points were collected by colorimeter testing to train and validate the ANN model. The accuracy of the trained and validated ANN model is compared to the AHRI 10-coefficient mapping, where the 10 coefficients are trained based on Equation (3) and listed in the work done by Ma et al., (2020). Regards to the 10-coefficient polynomial regression, 11 data points, i.e. least number of regression data points for least-square, have been selected wisely based on their locations within the compressor envelope. It is proposed by Ma et al., (2020) that the selection of the points, shown in Figure 2 started by choosing points on the boundary or vertices of the sketched compressor envelope, and then the other points are selected such that all the 11 points are evenly spread across the whole data set.

$$\begin{aligned}\dot{m}_{map}[\mathrm{kg/hr}] &= M_1 + M_2\cdot T_e + \mathrm{M}_3\cdot T_c + M_4\cdot T_e^2 + M_5\cdot(T_e\cdot T_c) + M_6\cdot T_c^2 + M_7\cdot T_e^3 + \mathrm{M}_8 \\ &\quad\cdot(T_e^2\cdot T_c) + M_9\cdot(T_e\cdot T_c^2) + M_{10}\cdot T_c^3 \\ \dot{W}_{map}[W] &= P_1 + P_2\cdot T_e + \mathrm{P}_3\cdot T_c + P_4\cdot T_s^2 + P_5\cdot(T_s\cdot T_d) + P_6\cdot T_d^2 + P_7\cdot T_s^3 + P_8\cdot(T_s^2\cdot T_d) + P_9 \\ &\quad\cdot(T_s\cdot T_d^2) + P_{10}\cdot T_d^3\end{aligned} \tag{3}$$

where T_e and T_c are evaporating and condensing temperatures in degree Celsius, respectively.

With respect to the ANN model, the architecture of the network is single-input-layer, single-hidden-layer and single-out-put layer to predict the mass flow rate and compressor power. In the first ANN model, the least number of training samples, i.e. five, are selected to train the network with 6 neurons in the single hidden layer. In the other ANN model, the training samples increase to 10 samples and another data point is chosen as testing point. All these 11 samples are the same data samples for 10-coefficiency polynomial regression. In addition, the neurons in the hidden layer are also increased to 12 in the second ANN model in order to match the expanded training data set. The connection between neurons of each layer in ANN models can be expressed as Equation (4).

$$y_k = \sum_{j=1}^{N_{neural}} (\omega_{kj}^{(2)}\varphi\left(\sum_{i=1}^{N_{input}} \omega_{ji}^{(1)}\cdot x_i + b_j^{(1)}\right) + b_k^{(2)}) \tag{4}$$

where x and y are the neural nods in input and output layers, respectively. $\omega_{ji}^{(1)}$ and $b_j^{(1)}$ are the weights and bias propagating the *i-th* input node to *j-th* neuron node in the hidden layer; and $\omega_{kj}^{(2)}$ and $b_k^{(2)}$ are the weights and bias propagating the *j-th* neuron node in hidden layer to *k-th* output node. A non-linear activation function $\varphi(\cdot)$, the hyperbolic tangent function is selected in the current work as activation function. Since the input and output variables are of different types and have different orders of magnitude, all inputs and outputs parameters are normalized by equation (Zendehboudi et al., 2017).

3.2 Uncertainty Analysis

Uncertainty of the compressor map output quantifies the potential difference between the true values of output to model predicted values of output. It starts from uncertainty of measurement values in both the model inputs and training data and propagates in the mathematical structure of compressor map or compressor ANN model. In current work, it is assumed that 10-coefficient mapping and ANN model

Based on uncertainty calculation method described in Cheung et al., (2018), the uncertainty of mass flow rate and compressor power due to inputs in 10-coefficient mapping are expressed in following equations.

$$\Delta\hat{\dot{m}}_r = \sqrt{\left(\frac{\partial\hat{\dot{m}}_r}{\partial T_e}\right)^2\cdot\Delta T_e^2 + \left(\frac{\partial\hat{\dot{m}}_r}{\partial T_c}\right)^2\cdot\Delta T_c^2} \tag{5}$$

$$\Delta\hat{\dot{W}}_{comp} = \sqrt{\left(\frac{\partial\hat{\dot{W}}_{comp}}{\partial T_e}\right)^2\cdot\Delta T_e^2 + \left(\frac{\partial\hat{\dot{W}}_{comp}}{\partial T_c}\right)^2\cdot\Delta T_c^2} \tag{6}$$

where T_e and T_c are dew-point temperatures which are calculated by the measured suction and discharge pressure.

The uncertainty of dew point temperature expressed in Equation (7) is formed as the uncertainty of pressure measurement ($\Delta P_{suc,mea}$, $\Delta P_{dis,mea}$) and uncertainty due to equation of state, since the dew-point temperatures are converted from measurements of suction and discharge pressure by the equation of state of the refrigerant.

$$\Delta T_e = \sqrt{\left(\frac{\partial T_e(P_{suc,mea})}{\partial P}\right)^2 \cdot (\Delta P_{suc,mea}^2 + \Delta P_{EOS}^2)}; \quad \Delta T_c = \sqrt{\left(\frac{\partial T_c(P_{dis,mea})}{\partial P}\right)^2 \cdot (\Delta P_{dis,mea}^2 + \Delta P_{EOS}^2)} \tag{7}$$

Uncertainty of pressure measurement (ΔP_{mea}) is usually described as a percentage uncertainty (listed in Table 1) of measurement value in the specification of a pressure transducer or thermocouple. And the uncertainty of dew-point pressure due to the equation of state is expressed by:

$$\Delta P_{EOS} = r_{EOS} P_{mea} \tag{8}$$

where r_{EOS} is the uncertainty associated with the equations of state which depends on the type of refrigerant. It is 0.5% of the dew point pressure for R410A.

Table 1: Sensor specifications

Sensor	Model	Range	Uncertainty
Thermocouple	Omega TMQSS-125T-6	0-350 C	0.75%
Pressure Transducer	Honeywell PX2AF1XX500PAAAX	0-500 psia/0-1000 psia	0.25%

According to JCGM GUM 100-2008 (JCGM, 2008), the combine uncertainty of outputs is obtained by appropriately combing the standard uncertainty of the input estimates. In ANN models, the uncertainty due to inputs can be calculated as follows:

$$\Delta \hat{m}_r = \sqrt{\begin{aligned}&\left(\frac{\partial \hat{m}_{comp}}{\partial T_{amb}}\right)^2 \cdot \Delta T_{amb,mea}^2 + \left(\frac{\partial \hat{m}_{comp}}{\partial P_{suc}}\right)^2 \cdot \Delta P_{suc,mea}^2 \\ &+ \left(\frac{\partial \hat{m}_{comp}}{\partial T_{suc}}\right)^2 \cdot \Delta T_{suc,mea}^2 + \left(\frac{\partial \hat{m}_{comp}}{\partial P_{dis}}\right)^2 \cdot \Delta P_{dis,mea}^2\end{aligned}} \tag{9}$$

$$\Delta \hat{W}_{comp} = \sqrt{\begin{aligned}&\left(\frac{\partial \hat{W}_{comp}}{\partial T_{amb}}\right)^2 \cdot \Delta T_{amb,mea}^2 + \left(\frac{\partial \hat{W}_{comp}}{\partial P_{suc}}\right)^2 \cdot \Delta P_{suc,mea}^2 \\ &+ \left(\frac{\partial \hat{W}_{comp}}{\partial T_{suc}}\right)^2 \cdot \Delta T_{suc,mea}^2 + \left(\frac{\partial \hat{W}_{comp}}{\partial P_{dis}}\right)^2 \cdot \Delta P_{dis,mea}^2\end{aligned}} \tag{10}$$

where the subscript *mea* represents a percentage uncertainty of measurement value. The partial derivative of an output with respect to an input shown in Equation (11) is calculated based on the neural network mathematical expression in Equation (4) with considering the nominalization process. In Equation (*11*), the capital X and Y represent the real measurement values of input and output, respectively; the small x and y represent the neural network inputs and outputs nominalized from measurement values.

$$\left(\frac{\partial\, Y(k)}{\partial\, X(i)}\right)^2 = \left(\sum_{j=1}^{N_{neural}} \left(\omega_{kj}^{(2)} \cdot \omega_{ji}^{(1)} \cdot \frac{\partial \varphi}{\varphi x(i)}\right) \cdot \frac{\mathrm{Y_{max}}(k) - \mathrm{Y_{min}}(k)}{\mathrm{X_{max}}(i) - \mathrm{X_{min}}(i)}\right)^2 \tag{11}$$

In ANN model, the input variables (temperature and pressure) are measured directly without converting by equation of state, the uncertainty due to state conversion are not be considered.

The other uncertainty components, such as uncertainty due to training data and uncertainty due to model random error, are not considered in this paper, since the model structure and model training methods are different between linear 10-coefficient mapping and non-linear ANN model.

2.3 Extrapolation Analysis

As aforementioned, the training samples for all three model are selected on the boundary or vertices of the sketched compressor envelope. However, the compressor envelope may not be rigorously identified in some cases that the model is necessary to predict the compressor performance beyond the range of training data set.

Thus, extrapolation analysis is conducted here to investigate the issue of compressor map performance outside the range of the training data set. Different from the previous case, the new training points in Figure 2 are selected inside the compressor envelope to avoid choosing data points located on the boundary or vertices of the sketched compressor envelope. The data points outside the training data set are validation data points for extrapolation capabilities analysis.

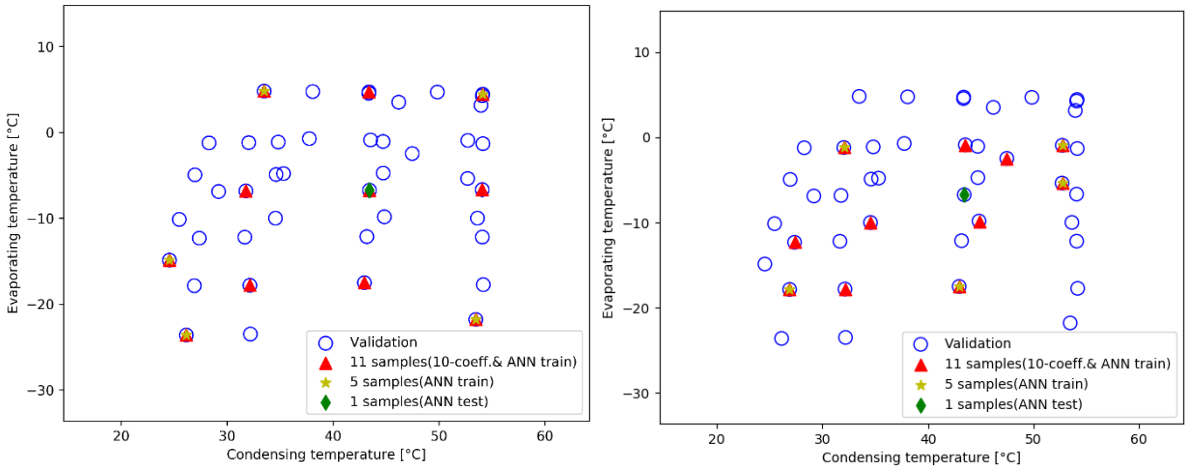

Figure 2: Compressor map with training data: (a) training data selected on compressor envelope (b) training data selected within compressor envelope

4. RESULTS

To investigate the accuracy of the ANN model, a set of parity plots of are utilized to compare the 10-coefficient polynomial model and the ANN models with variable number of training samples. It is evident from Figure 3 and Figure 4 that 10-coefficient polynomial and ANN models can predict the compressor performance reasonably well. By looking at the parity plots in Figure 3, the mass flow rate is predicted by the 10-coefficient polynomial model with a $MAPE$ of 0.83% and R^2 of 99.85%, and power ouput reported a $MAPE$ of 0.26% and R^2 of 99.96%. By comparing the two ANN models, the one trained with 5 experimental samples presents a slightly larger $MAPE$ value of 2.85% and lower R^2 of 99.07%. However, the ANN model trained with 10 samples shows as high accuracy as the 10-coefficient polynomial model with a $MAPE$ of 0.75% and R^2 of 99.88%. With respect to compressor power prediction in Figure 4, both 10-coefficient polynomial and ANN model trained by 10 samples presents a good regression that nearly all data points fall on the best-fitting line with only 0.25% and 0.34% of $MAPE$ respectively. Only the ANN model trained by 5 samples report a slightly large $MAPE$ of 1.42%.

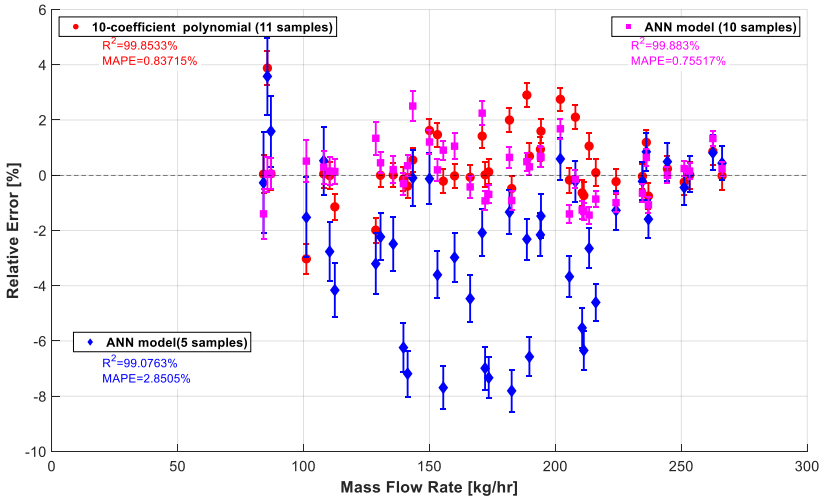

Figure 3: Comparison of validating data between models and experiment for mass flow rate (Models trained by the samples on the boundary of the compressor envelope)

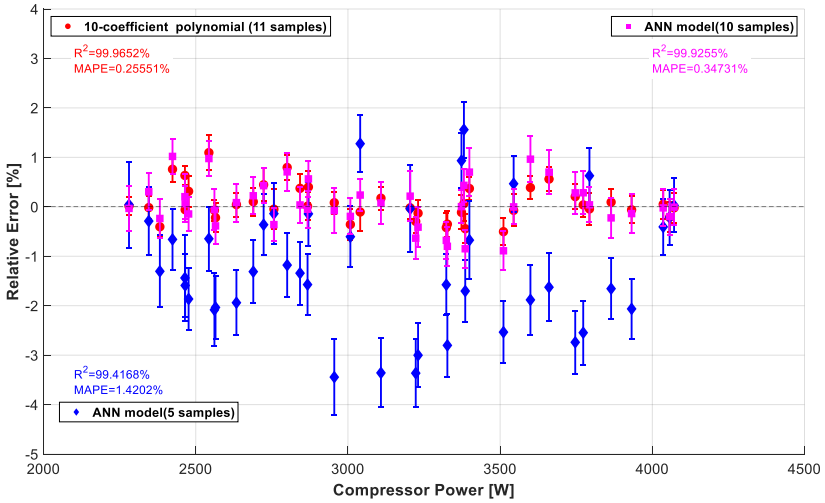

Figure 4: Comparison of validating data between models and experiment for compressor power (Models trained by the samples on the boundary of the compressor envelope)

Furthermore, the uncertainties of mass flow rate and compressor power for each data sample are represented as error bars in Figure 3 and Figure 4. In Figure 3, the ANN model trained by 5 samples has longer error bars in comparison to that in the 10-coefficient map and in ANN model trained by 10 samples, which means that the uncertainties of the ANN model trained by 5 samples are the largest among the three models in the prediction of mass flow rate. Similar results are represented in Figure 4 for compressor power prediction. It illustrates that the ANN model trained by 5 samples has larger model prediction errors and uncertainties compared with the other two models.

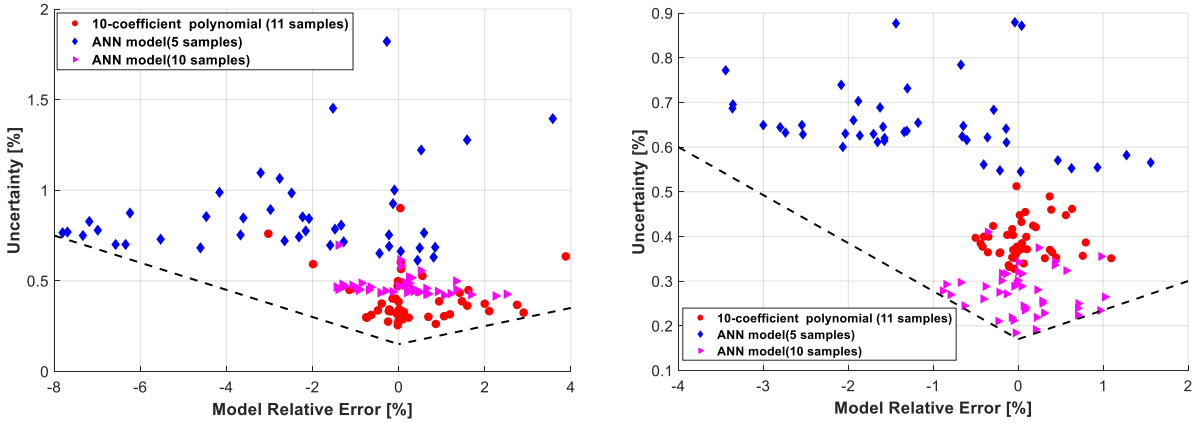

(a) Mass Flow Rate (b) Compressor Power

Figure 5: Uncertainty errors with model accuracy of all data samples (Models are trained by the samples on the boundary of the compressor envelope)

Figure 5 is plotted to investigate how uncertainty changes with model accuracy. In general, it shows that the larger the model relative error is, the higher uncertainty the model has, which means uncertainties increase with a decrease of model accuracy. In Figure 5, it is clearer to see that the ANN model trained by 5 samples represents highest uncertainty and lowest model accuracy for both mass flow rate and compressor power. In comparation ANN model with 10-coefficiency map, the ANN model with 10 training samples has higher uncertainties but lower model relative errors in the prediction of mass flow rate; but has lower uncertainties and larger model relative errors in the prediction of compressor power. In 10-coefficiency map and two ANN models, since there are several data points have lower relative error but higher uncertainties, the definite relationship between model accuracy and uncertainty cannot be identified in the current work.

Figure 6 and Figure 7 represent the model accuracy of 10-coefficiency map and two ANN models with training data samples locating inside the sketched compressor envelope. In comparation Figure 6 to Figure 3 for mass flow rate prediction, the R^2s for three models, which are 10-coefficiency polynomial, ANN model trained by 5 samples and ANN model trained by 10 samples, reduce to 98.58%, 99.56% and 98.97% respectively; the *MAPE*s increase to 2.53%, 3.73% and 3.02% respectively. In other words, all three models are not as accurate as before when the predicting data points are selected beyond the training data set. This trend also happens on compressor power prediction. In Figure 7, the R^2s slightly decrease to 99.63%, 99.26% and 97.06%, the *MAPE*s clime up to 0.63%, 1.19% and 2.44% respectively for 10-coefficient map, ANN model trained by 5 samples and ANN model trained by 10 samples.

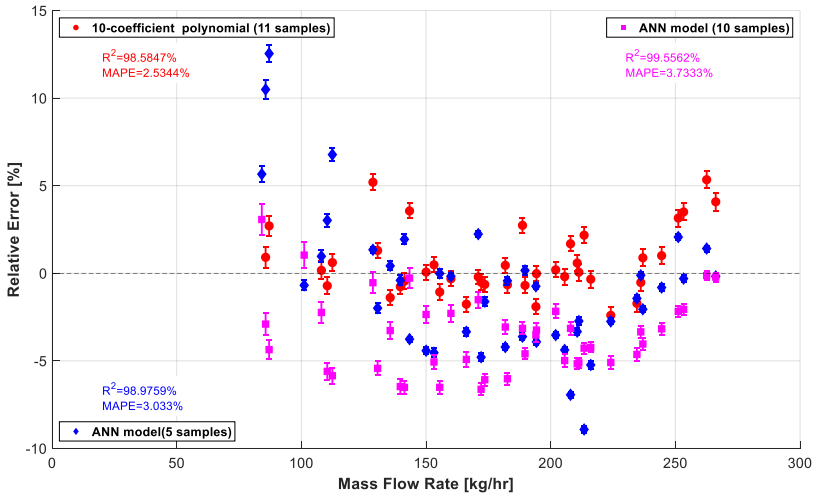

Figure 6: Comparison of validating data between models and experiment for mass flow rate (Models trained by samples inside compressor envelope)

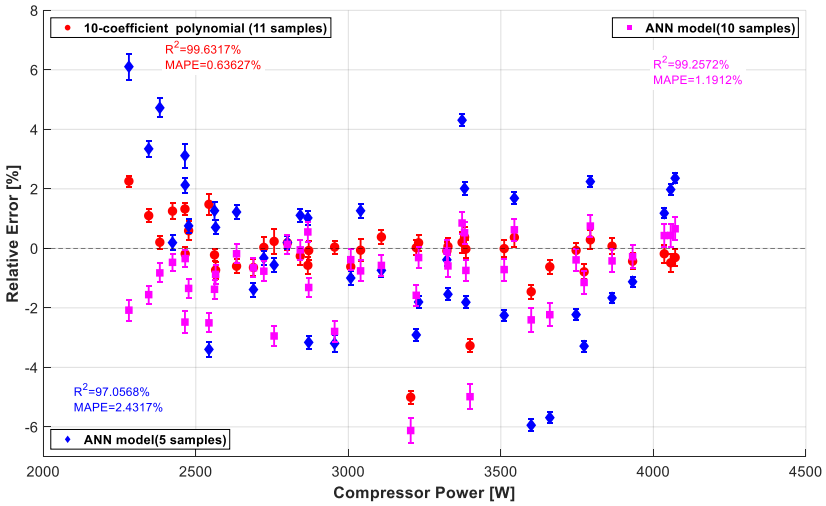

Figure 7: Comparison of validating data between models and experiment for compressor power (Models are trained by samples inside compressor envelope)

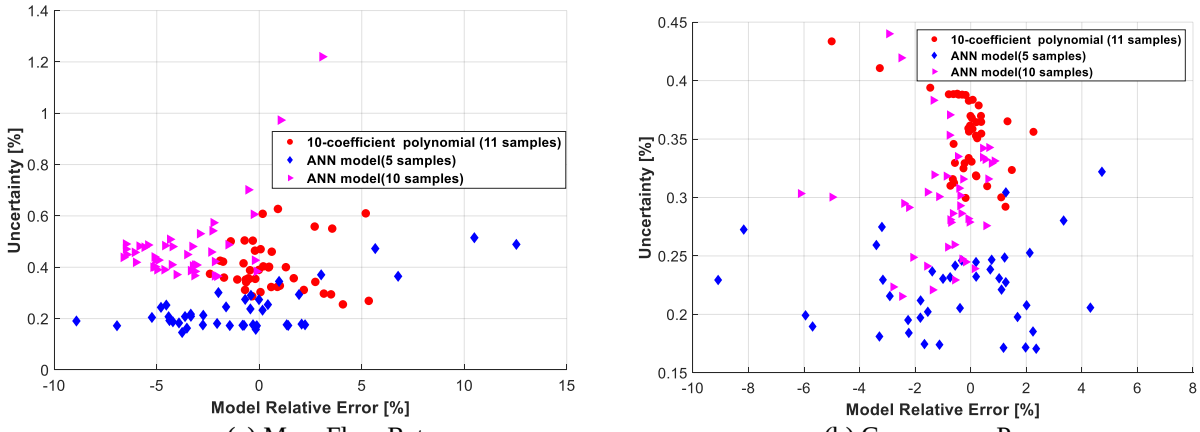

(a) Mass Flow Rate (b) Compressor Power

Figure 8: Uncertainty errors with model accuracy of all data samples (Models are trained by samples inside compressor envelope)

Figure 8 shows the relationship between the model relative error and uncertainty for 10-coefficiency map and two ANN models when the range of training samples is much smaller than compressor envelope. Comparing to Figure 5, the uncertainties of ANN model with 5 training samples are much lower than before. In contrast to ANN model with 5 training samples, the uncertainties of 10-coefficient polynomial and ANN model with 10 training samples are roughly equal to

the uncertainties presented in Figure 5. Furthermore, in Figure 8, no obvious correlations is observed between the model predictive errors and uncertainty errors.

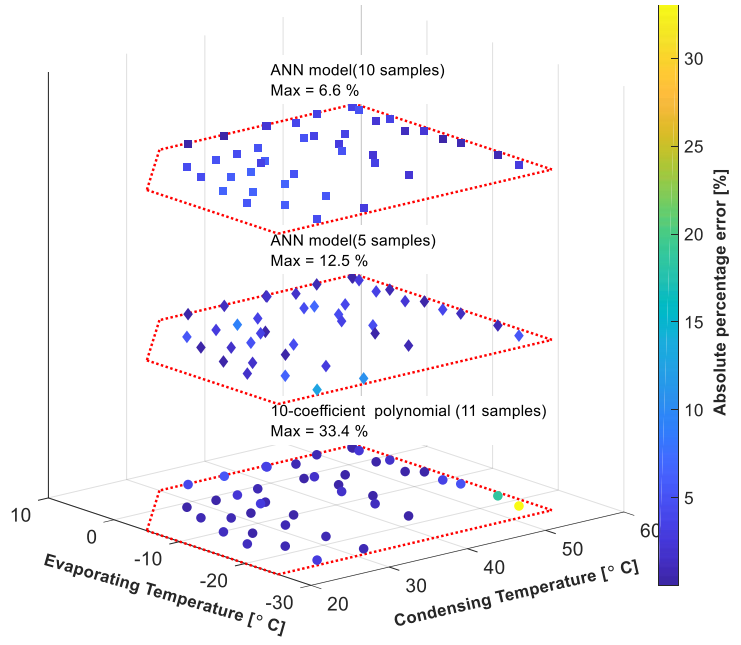

(a)

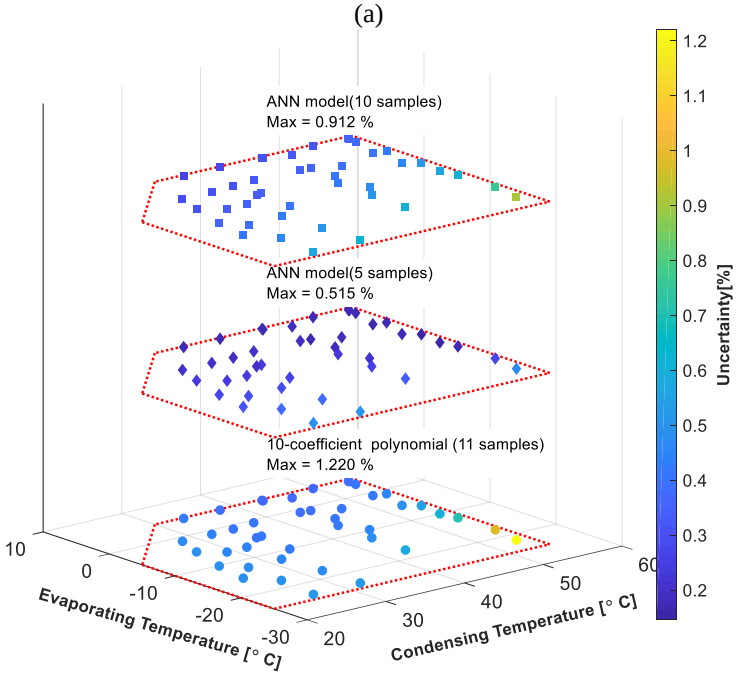

(b)

Figure 9: Absolute percentage errors and uncertainty errors of mass flow rate for all validating points of the compressor map (Models are trained by samples inside compressor envelope)

Table 2: Absolute percentage error comparison of models with different training data set

	Training samples on compressor envelope		Training samples within compressor envelope	
	Mass Flow Rate	Compressor Power	Mass Flow Rate	Compressor Power
ANN model (10 training samples)	2.5%	1.0%	6.6%	6.1%
ANN model (5 training samples)	7.8%	3.4%	12.5%	9.1%
10-Coefficient polynomial	3.9%	1.1%	33.4%	5.0%

To clearly locate the position of data samples representing larger model relative error or higher uncertainty, the plots in Figure 9 and Figure 10 represent the absolute percentage error (*APE*) and model uncertainty of mass flow rate and compressor power for each data point and their deviation distribution on compressor map when the range of model training data set is smaller than the range of validation data set. Overall, the maximum *APE*s shown in Figure 9 and Figure 10 for three models increase significantly in comparation of the corresponding results presented in Ma et al., (2020).

With respect to mass flow rate prediction, Table 2 illustrates that the maximum APE obtained by 10-coefficient map dramatically increases from 3.9% to 33.4%, where the corresponding data point shown in Figure 9(a) is on the right bottom vertex of the sketched compressor map. The data points representing maximum model prediction error is also the data point has highest uncertainty as shown in Figure 9(b). Furthermore, the maximum *APE*s for the ANN model with 10 training samples and the ANN model with 5 training samples also increase from 2.5% to 6.6%, and from 7.8% to 12.5% respectively summarized in Table 2. It also can be observed in the ANN models that the data points with higher *APE*s have higher uncertainties, where located on the vertices or boundary lines of the compressor map.

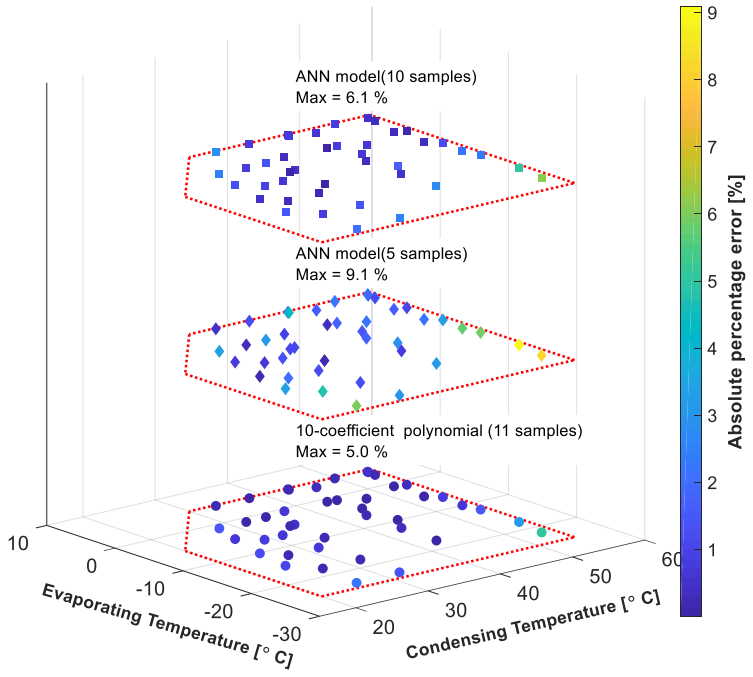

(a)

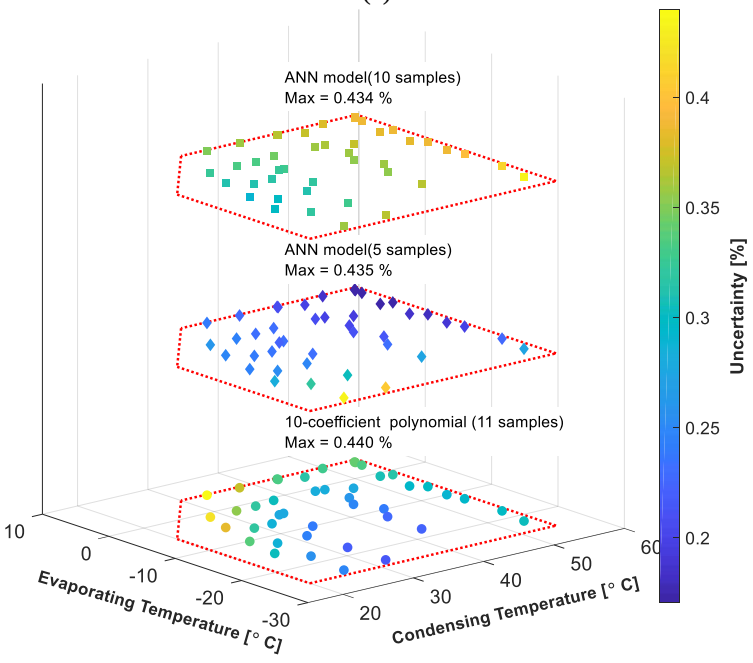

(b)

Figure 10: APEs of compressor power for all validating points of the compressor map (Models are trained by samples within compressor envelope)

To compare *APE*s in compressor power prediction summarized in Table 2, the maximum *APE*s for three models, i.e. 10-coefficiency mapping, ANN model with 5 training samples and ANN model with 10 training samples, increase from 1.1% to 5.0%, 3.4% to 9.1% and 1.0% to 6.1% respectively. It can be observed in Figure 10 that the data points showing higher *APE*s are the points having higher uncertainties, where located along the boundary lines of compressor map.

It can conclude that when the range of training data set is smaller than the compressor envelope, the model is less accurate and the uncertainty due to inputs is higher, the data points representing lower accuracy and higher uncertainty are the points beyond the range of the training data set.

5. CONCLUSIONS

In summary, the automated compressor performance mapping methodology based on ANN modeling with various training data set is implemented on a hermetic dual-cylinder rolling-piston compressor. And the accuracy and reliability of the proposed methodology are compared to the conventional 10-coefficient polynomial mapping, and the propagated uncertainties through the model and model extrapolation capabilities are also analyzed in this paper. It can conclude that the ANN model with 10 training samples has small relative error and low uncertainty when the training samples are chosen on vertex or boundary line of compressor map. With a little extrapolation, the accuracy of three models decrease and the uncertainty of ANN models also decrease.

Nomenclature

T_{amb}	Ambient temperature [℃]	P_{suc}	Suction pressure [kPa]
T_{suc}	Suction temperature [℃]	P_{dis}	Discharge pressure [kPa]
T_{dis}	Discharge temperature [℃]	$\dot{m}_r$	Mass flow rate of refrigerant [kg/hr]
$\dot{W}_{comp}$	Compressor power consumption [W]	T_e	Evaporating temperature [℃]
T_c	Condensing temperature [℃]	ω	weights
b	bias	x	Input node in ANN
y	Output node in ANN	X	Input quantity
Y	Output quantity	r	Uncertainty error
EOS	Equation of state		

References

AHRI. (2015). *NATIONAL STANDARD CAN / ANSI / AHRI 540-2015 , Performance Rating of Positive Displacement Refrigerant Compressors and Compressor Units*.

Aute, V., Martin, C., & Radermacher, R. (2015). AHRI Project 8013 : A Study of Methods to Represent Compressor Performance Data over an Operating Envelope Based on a Finite Set of Test Data. *Air-Conditioning, Heating, and Refrigeration Institute*.

Cheung, H., Sarfraz, O., & Bach, C. K. (2018). A method to calculate uncertainty of empirical compressor maps with the consideration of extrapolation effect and choice of training data. *Science and Technology for the Built Environment*, *24*(7), 743–758. https://doi.org/10.1080/23744731.2017.1372805

JCGM. (2008). Evaluation of measurement data — Guide to the expression of uncertainty in measurement. *International Organization for Standardization Geneva ISBN*, *50*(September), 134. http://www.bipm.org/en/publications/guides/gum.html

Ma, J., Ding, X., Horton, W. T., & Ziviani, D. (2020). Development of an automated compressor performance mapping using artificial neural network and multiple compressor technologies. *International Journal of Refrigeration*, *120*, 66–80. https://doi.org/10.1016/j.ijrefrig.2020.08.001

Zendehboudi, A., Li, X., & Wang, B. (2017). Utilisation des modèles ANN et ANFIS pour prédire un compresseur à spirale à vitesse variable avec injection de vapeur. *International Journal of Refrigeration*, *74*, 473–485. https://doi.org/10.1016/j.ijrefrig.2016.11.011

Ziviani, D., Bahman, A., & Groll, E. (2019). *Multi-input multi-output (MIMO) artificial neural network (ANN) models applied to economized ccroll compressors*. *2016*. https://doi.org/10.18462/iir.icr.2019.1321

Acknowledgements

The authors would like to thank the Center for High Performance Buildings (CHPB) for the financial support to this project (project number CHPB-39).